

THE PENNSYLVANIA STATE UNIVERSITY
SCHREYER HONORS COLLEGE

DEPARTMENT OF MECHANICAL AND NUCLEAR ENGINEERING

**THE EFFECT OF STATOR AND ROTOR FORM ERROR ON AIR BEARING
SPINDLE ACCURACY**

JAMES NEVEL
SPRING 2011

A thesis
submitted in partial fulfillment
of the requirements
for a baccalaureate degree
in Mechanical Engineering
with honors in Mechanical Engineering

Reviewed and approved* by the following:

Eric Marsh
Professor of Mechanical Engineering
Thesis Supervisor

James G. Brasseur
Professor of Mechanical Engineering, Bioengineering,
and Mathematics
Honors Adviser

Karen A. Thole
Department Head of Mechanical and Nuclear
Engineering
Faculty Reader

* Signatures are on file in the Schreyer Honors College.

ABSTRACT

The error motion of an air bearing reflects the interaction between the spinning rotor and stator components' form errors through the pressurized air film. Due to the nature of the machining and production process of rotor and stator components, long-wavelength geometric flaws, known as form errors, can be found on the air bearing surfaces. These form errors can be an influence to the operation of the spindle and are suspected to be causes of a decrease in spindle accuracy. An exploration of the effects of these surface flaws in relation to spindle accuracy will be done through calculation and simulation. Geometric errors in the rotor and stator of a high precision spindle were modeled using a discretized set of stiffness elements interacting with non-round stator and rotor surfaces. A complete outline of the equations used to determine the spindle error is included. The governing equation was formulated to map the x and y components of the spindle error during operation by minimizing the potential energy stored in the air film. We investigated the process of incorporating lobing into the rotor and stator to reduce error from geometric manufacturing flaws to increase precision and accuracy through a theoretical approach. It was determined that lobe designs in the rotor and stator will not affect spindle performance due to the smoothing effect of the air during spindle operation.

TABLE OF CONTENTS

| | |
|---|-----|
| LIST OF FIGURES | iii |
| LIST OF TABLES..... | iv |
| ACKNOWLEDGEMENTS..... | v |
| Chapter 1 Introduction | 1 |
| 1.1 Overview of High Precision Spindles..... | 3 |
| 1.2 Geometric Form Errors | 6 |
| 1.3 Rotor/Stator Design Implementation | 8 |
| 1.4 Simulation | 9 |
| Chapter 2 Governing Equations for Spindle Error Motion..... | 9 |
| 2.1 Definition of Variables..... | 10 |
| 2.2 Minimizing Energy | 10 |
| 2.2.1 X Component Minimization | 11 |
| 2.2.2 Y Component Minimization | 13 |
| Chapter 3 Data Generation and Analysis..... | 15 |
| 3.1 Creating and Array for Rotation | 15 |
| 3.2 Summation of $R(\theta)\cos(\theta)$ and $r(\alpha-\theta)\cos(\theta)$ | 16 |
| 3.3 Summation of Assorted Trigometric Functions | 18 |
| Chapter 4 Discussion of Results | 19 |
| 4.1 Summation Calculations | 20 |
| 4.2 Non-linear Spring Behavior | 21 |
| 4.3 Load of Air Bearing | 21 |
| 4.4 Further Reccomendations..... | 22 |
| 4.5 Conclusion | 22 |
| References..... | 24 |

LIST OF FIGURES

| | |
|--|----|
| Figure 1-1: Artifacts for measuring spindle performance (after Marsh, 2008)..... | 1 |
| Figure 1-2: Surface Flaws on turbine rotor..... | 2 |
| Figure 1-3: Capacitive sensor measurement using a lapped steel artifact (after Marsh, 2008) | 3 |
| Figure 1-4: Measurements of spindle error (after Marsh, 2008)..... | 4 |
| Figure 1-5: Internal boring surface finish (after Schalcosky, 2004) | 5 |
| Figure 1-6: Repeatability in spindle error motion measurement (after Couey, 2006) | 6 |
| Figure 1-7: Error motion in x , y , and z directions (after Grejda, 2003) | 7 |
| Figure 1-8: Exaggerated cross section of a four lobe air bearing stator..... | 8 |
| Figure 4-1: Stator design with multiple lobes..... | 19 |

LIST OF TABLES

| | |
|---|----|
| Table 3-1: Rotation array creation in Excel..... | 16 |
| Table 3-2: $R(\theta)\cos\theta$ and $r(\alpha-\theta)\cos\theta$ | 17 |

ACKNOWLEDGEMENTS

I'd like to thank Dr. Eric Marsh for providing me with this opportunity to further my educational experience in the field of Mechanical Engineering. He was able to provide motivation through ME360 that sparked my interest in machine design and has been a great asset to the formulation of my thesis. I would also like to thank Dr. James Brasseur for the assistance that he provided through advising this past semester. Finally, I would like to thank Dr. Matthew Mench for assisting me through the preliminary thesis requirements in the spring of 2010.

Chapter 1

Introduction

With the extreme accuracy provided by high precision air bearing spindles, they are able to be used in micro-machining operations and provide a very fine surface finish. When measuring the radial error motion of a spindle rotating at high speeds, the accuracy can be within nanometers from the axis of rotation. Artifacts shown below in Fig. 1-1 allow for high precision measurements to be made during spindle operation. Capacitive sensors are used to measure displacements in the x , y , and z directions. The error that this research will focus on is radial motion.

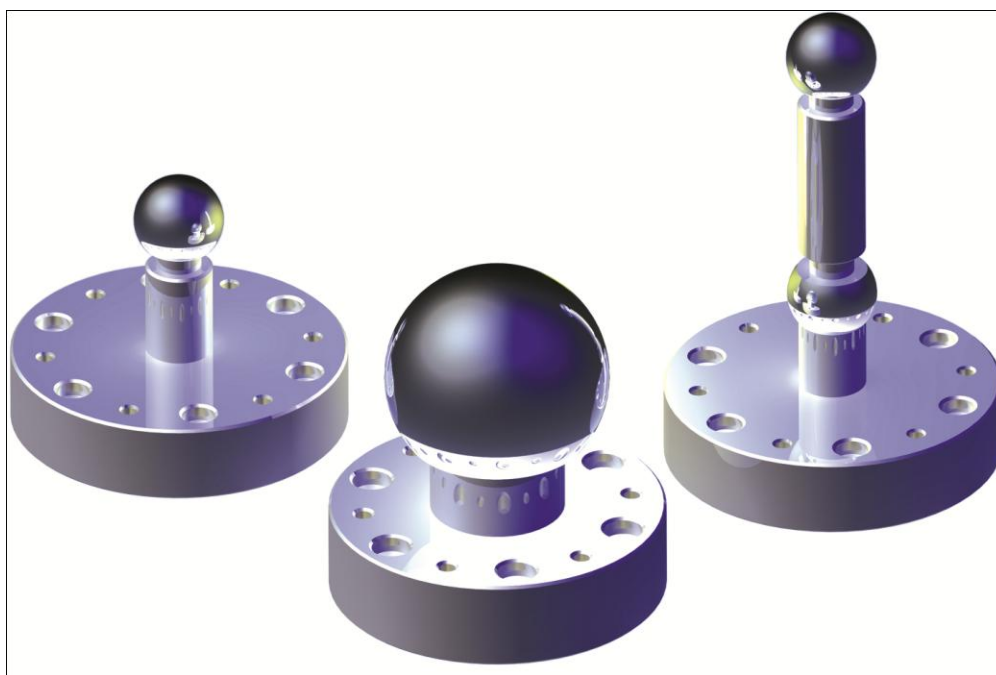


Figure 1-1: Artifacts for measuring spindle performance (after Marsh, 2008).

By investigating some of the geometric limitations in creating components such as the rotor and stator for the spindle construction, we have gained further insight into increasing the accuracy to allow for even higher precision. Due to imperfect lathe and grinding operations, flaws such as scratches and imperfections in the roundness of the rotor and stator are unavoidable during production, as shown in Fig. 1-2. These geometric flaws on the components of the spindle affect the performance of the spindle during operation.

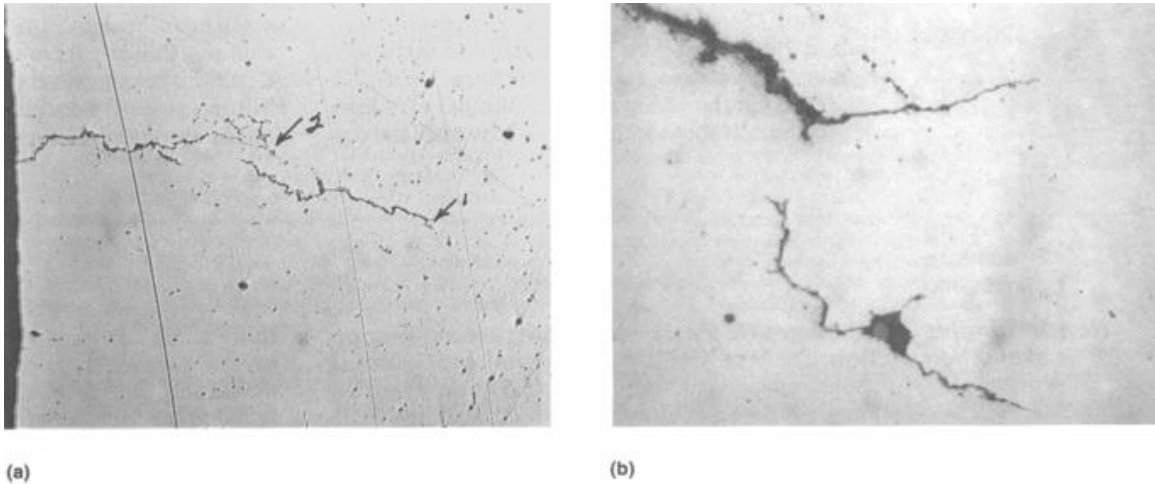


Figure 1-2: Surface flaws on turbine rotor.

The main parts of the spindle that were investigated throughout this analysis are the rotor, the stator, and the externally-pressurized air film between the two. The objective of this investigation is to account for form error in spindle components by modeling a lobed shape into the rotor and stator and calculated the effect on spindle error motion. Provided below is an overview on the operation of air bearing spindles, required equations to simulate spindle operation, methods of data analysis using Microsoft Excel, and a discussion of results with future recommendations.

1.1 - Overview of High Precision Spindles

A spindle allows high accuracy rotation between components while providing stiffness and load capacity. The three components that make up a spindle are the rotor, stator, and the bearings.

The focus of this study is on air bearing spindles, but other spindles use rolling element bearings to achieve the same result. Ideally, the spindle will only allow motion in one degree of freedom and that is pure rotation. Motion in any other direction is called spindle error motion. The error and precision are measured using capacitive sensors to provide high resolution (1nm) and high bandwidth (greater than 10 kHz).

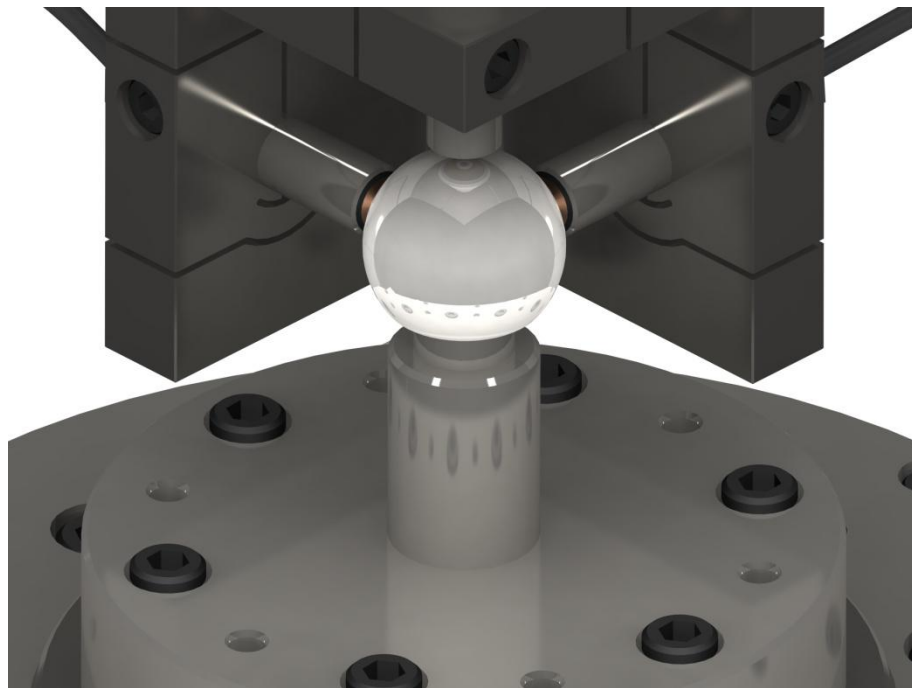


Figure 1-3: Capacitive sensor measurement using a lapped steel artifact (after Marsh, 2008).

Fig. 1-3 shows the method used for testing spindle accuracy using an artifact and three capacitive sensors. The sensors are able to determine displacement in the normal direction with sub-nanometer accuracy.

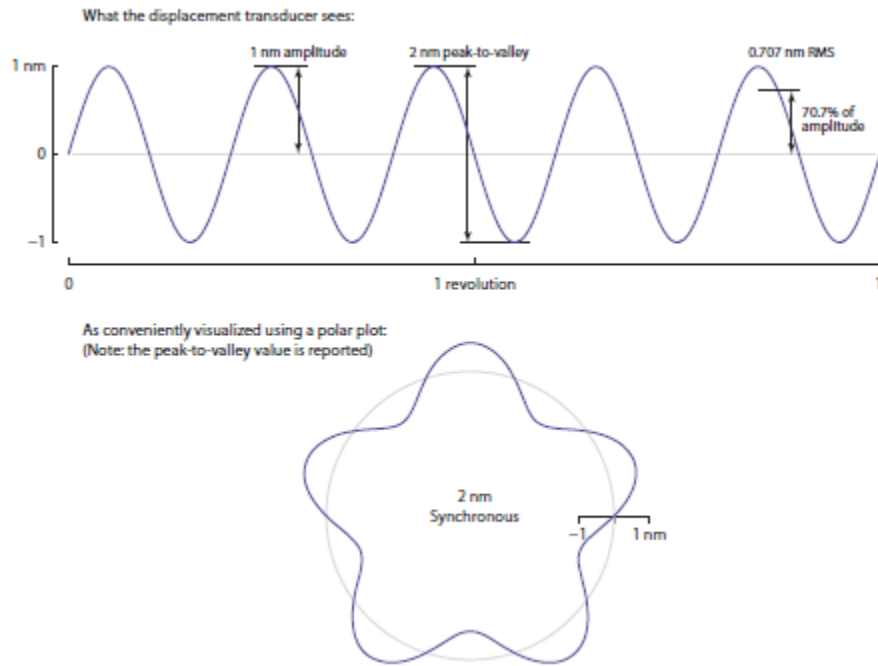


Figure 1-4: Measurements of spindle error (after Marsh, 2008).

Fig. 1-4 shows a representative five-lobe error that could come from a spindle found on equipment such as a CNC diamond turning lathe. It can be seen that the spindle does not rotate in a perfectly circular fashion, but there undesirable off-axis motion of an amplitude of 2nm. Fig. 1-5 shows an application of high precision spindles being used to generate a very round and smooth internal surface. By eliminating error in the rotational (radial) direction of the spindle, the ability to produce finer surface finishes is increased.

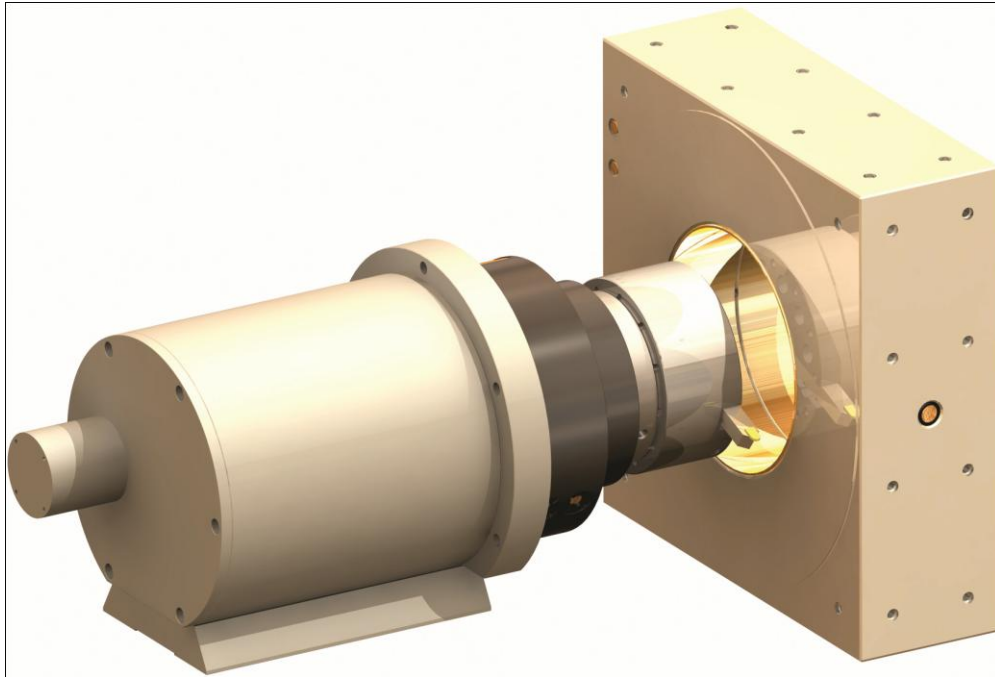


Figure 1-5: Internal boring surface finish (after Schalcosky, 2004).

Spindle error motion measurements are also used to assess the spindle's repeatability. Increased repeatability signifies a more precise instrument. Fig. 1-6 illustrates results from ten consecutive trials for displacements measurement. The results show sub-nanometer repeatability. The artifact was also measured in order to compare the errors found in spindle operation with the slight imperfections of the artifact.

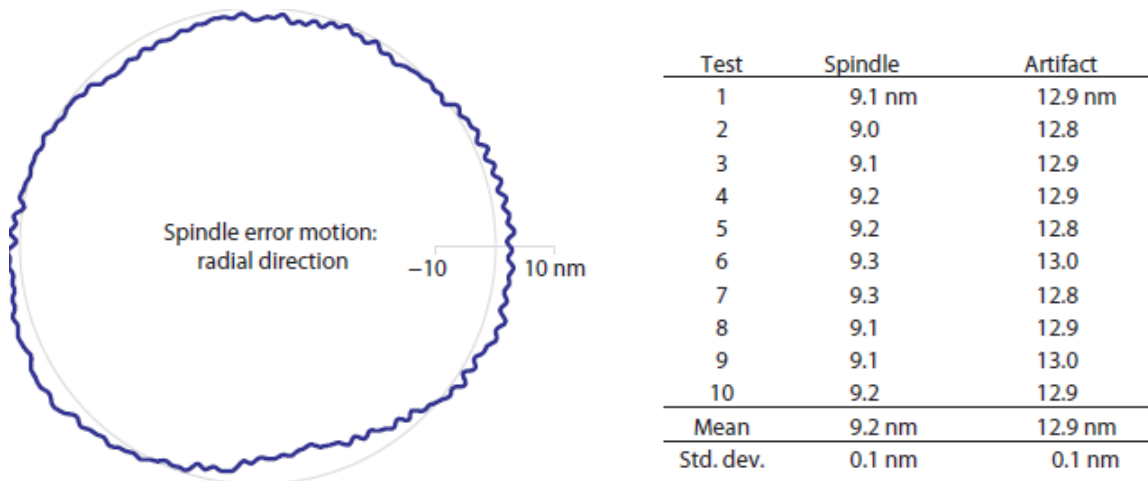


Figure 1-6: Repeatability in spindle error motion measurement (after Couey, 2006).

1.2 - Geometric Form Errors

The rotor and the stator are machined to a tolerance that can be less than a few micrometers.

However, the precision of the spindles has been measured to be within a few nanometers.

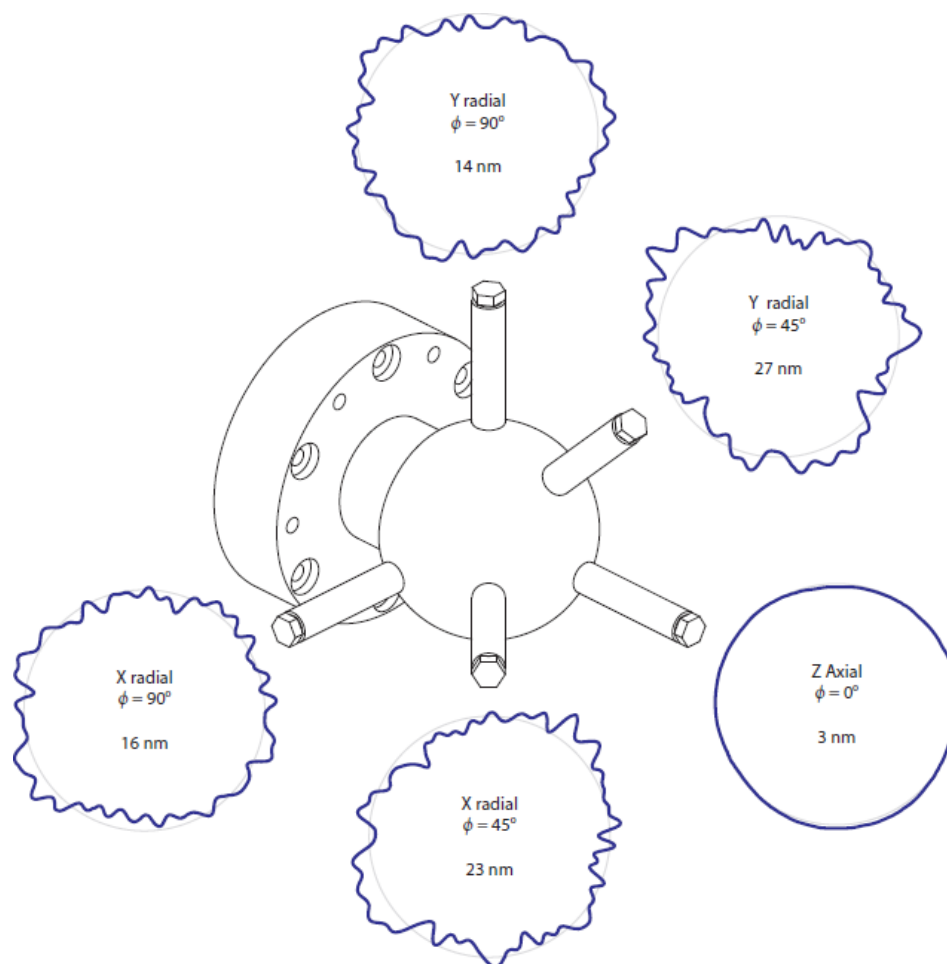


Figure 1-7: Error motion in x , y , and z directions (after Grejda, 2003).

Fig. 1-7 illustrates the magnitude of error motions found in air bearing spindles. It can be seen that the error motion is anywhere from about 5 to 25nm, depending on the measurement orientation. These very small numbers can be compared to the individual components' form error that is in the 1 to 2 micron range. This huge smoothing effect is a result of the high pressure air that absorbs most of the flaws encountered on the rotor and stator. The air acts as a distributed spring and greatly reduces the impact of surface flaws between the components. In this analysis, the elasticity of the air was modeled using discrete linear springs spaced every degree between the rotor to the stator. By modeling the rotor and stator form errors to incorporate lobing, flaws

from machining introduced into the model to explore their effect on spindle accuracy.

1.3 - Rotor/Stator Design Implementation

Fig. 1-8 shows a greatly exaggerated four lobe geometric form error that could be found on an air bearing component. In practice, the lobes would be clearly be much shallower than the shape shown here. In this work, different combinations of lobes on the rotor and stator were investigated. The possibility could be that both components have the same number of lobes or they could differ from one another. For example, the rotor could have five lobes while the stator has mostly six-lobe form error.

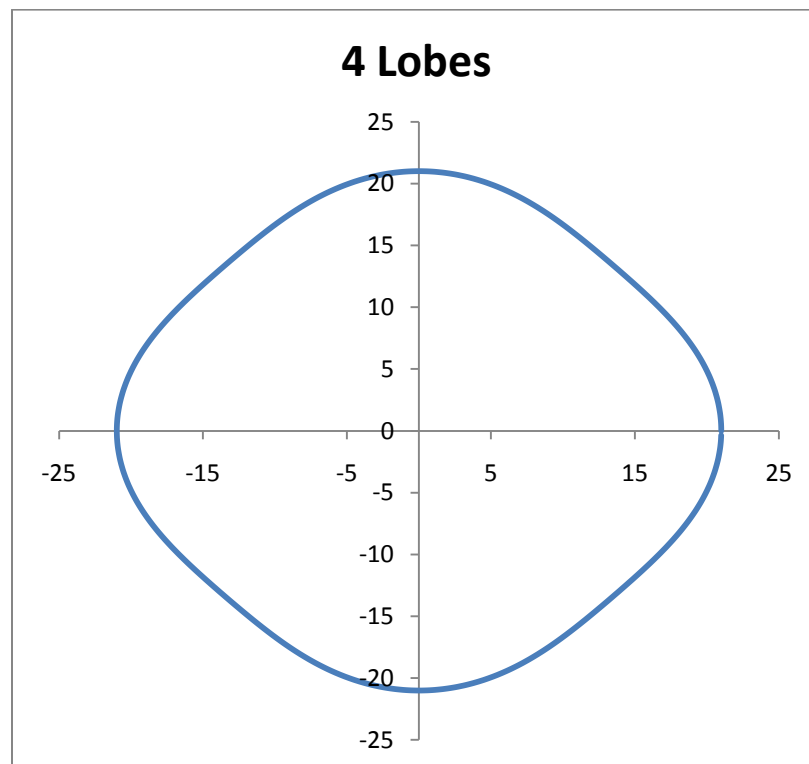


Figure 1-8: Exaggerated cross section of a four lobe air bearing stator.

1.4 - Simulation

The simulation work was done using Microsoft Excel. The data were generated through the implementation of governing equations that will be shown in Chapter 2. The spreadsheet will perform all necessary calculations to simulate the motion of a spindle's axis of rotation. The user may modify the outer diameter (OD) of the rotor and the inner diameter (ID) of the stator as well as the lobe shapes of both components. The spreadsheet calculated the location of axis of rotation of the spindle through one full rotation.

Chapter 2

Governing Equations for Spindle Error Motion

Chapter 2 outlines all of the variables that were used to calculate the position of the center of the spindle. Also, the full derivation process for determining the x and y components of the axis of rotation are provided. The aim of Chapter 2 is to provide a full understanding of the governing equations for spindle error motion through a step by step derivation process. The equations derived in Chapter 2 will be used in the construction of the simulation in Microsoft Excel to explore the effect of various lobe designs in the rotor and stator.

2.1 - Definition of Variables

R was defined as the radius of the stator (out radius) and is the function:

$$R = A\sin(n\theta) \quad (1)$$

The variable r was defined as the radius of the rotor (inner radius) and was used as the function:

$$r = B\sin(m\theta) \quad (2)$$

In both cases, n and m represent the number of lobes on radial surface. The linear spring constant provided by the air bearing was represented as variable k . The calculation seeks to minimize the potential energy in the distributed springs by allowing the rotor to move with respect to the stator in the x and y directions. The results were computed for various values of variables m and n in the functions defined in Eq. 1 and Eq. 2 above. θ represented the orientation angle of the rotor and stator. This was used in the creation of the angular-dependent deflection between both components. α represented the rotation of the stator inside the rotor. Both θ and α ranged from 0 to 2π capture a full spindle rotation.

2.2 - Minimizing Energy

The minimization of energy of the system provides the best possible positions of the center of the spindle through a full rotation. The equation used to analyze the energy of the system is:

$$E = \sum_{i=0}^{359} \frac{1}{2} k [R(\theta) - r(\theta - \alpha) - x \cos \theta - y \sin \theta]^2 \quad (3)$$

This equation represents the total energy storage within the collection of springs. It also takes account of the position-dependent radii of both the stator and rotor. By setting the partial derivative of Eq. 3 with respect to x equal to zero, we may compute the x components of the spindle through a full rotation. The same was done in the y direction. In Eq. 3, the $(\theta - \alpha)$ term represents the rotation of the rotor inside the stator. Each time α increases by one degree, the results were recalculated to provide the new x and y values for the center of the spindle.

2.2.1 - X Component Minimization

The x components for minimization of energy can be found by taking the partial derivative of Eq. 3 with respect to x and setting this derivative equal to zero.

$$0 = \sum_{i=0}^{359} \frac{1}{2} k 2[R(\theta) - r(\theta - \alpha) - x \cos \theta - y \sin \theta] \cos \theta \quad (4)$$

It is important to note that in Eq. 4 that R and r both contain the sine function. When the equation is simplified, the spring constant k will be cancelled from the equation. This will leave a simplified form of Eq. 4.

$$\sum_{i=0}^{359} R(\theta) \cos \theta - \sum_{i=0}^{359} r(\theta - \alpha) \cos \theta - \sum_{i=0}^{359} x \cos^2 \theta - \sum_{i=0}^{359} y \sin \theta \cos \theta = 0 \quad (4a)$$

The components of Eq. 4 show that each term will contain a summation. Eq. 4 was arranged again to make it easier to solve for the x components.

$$a_1 = \sum_{i=0}^{359} R(\theta) \cos \theta - \sum_{i=0}^{359} r(\theta - \alpha) \cos \theta \quad (4b)$$

Eq. 4b was recorded as one variable named a_1 . This made the math easier to follow by utilizing one variable instead of a full equation.

$$b_1 = \sum_{i=0}^{359} x \cos^2 \theta \quad (4c)$$

Eq. 4c was recorded as a new variable called b_1 . Again, this made the simplification of Eq. 4 much easier to follow.

$$c_1 = \sum_{i=0}^{359} y \sin \theta \cos \theta \quad (4d)$$

Finally, Eq. 4d was represented by the variable c_1 .

Now that the variables have all been defined, obtaining a final equation to solve for the x components was possible. Eq. 4 was rearranged and simplified as a function of x and y , and the new variables defined in equations 4b-4d.

$$x b_1 + y c_1 = a_1 \quad (5)$$

Eq. 5 was simplified with one additional step to remove the y components because the summation of a $\sin \theta \cos \theta$ around a full rotation will yield zero.

$$x = \frac{a_1}{b_1} \quad (5a)$$

This equation allows calculation of the x components for mapping the location of the center of the spindle. This equation was used during the analysis on Excel to capture all of the summations around the rotor and the stator.

2.2.2 - Y Component Minimization

The y components for minimization of energy can be found by taking the derivative of Eq. 3 with respect to y and setting that derivative equal to zero. The following process is very similar to the process that was done with the simplification of x components.

$$0 = \sum_{i=0}^{359} \frac{1}{2} k * 2[R(\theta) - r(\theta - \alpha) - x \cos \theta - y \sin \theta] \sin \theta \quad (6)$$

Eq. 6 is identical to Eq. 4 with the exception that a $\sin \theta$ replaces the $\cos \theta$ found in Eq. 4. Similar to Eq. 4, the spring constant k will be dropped from the equation. This will leave a simplified form of Eq. 6.

$$\sum_{i=0}^{359} R(\theta) \sin \theta - \sum_{i=0}^{359} r(\theta - \alpha) \sin \theta - \sum_{i=0}^{359} x \sin \theta \cos \theta - \sum_{i=0}^{359} y \sin^2 \theta = 0 \quad (6a)$$

Much like what was done to the analysis of the x components, each term can now easily be seen with a summation. Eq. 6a was written in terms of new variables to make it easier to follow.

$$a_2 = \sum_{i=0}^{359} R(\theta) \cos \theta - \sum_{i=0}^{359} r(\theta - \alpha) \cos \theta \quad (6b)$$

Eq. 4b was recorded as one variable named a_2 . In terms of variables, Eq. 6b is exactly the same as Eq. 4b, which means that $a_1 = a_2$.

$$b_2 = \sum_{i=0}^{359} x \sin \theta \cos \theta \quad (6c)$$

Equation 6c was recorded as a new variable called b_2 . This is very similar to the variable c_1 from the previous analysis except that the y has been replaced with an x in Eq. 6c.

$$c_2 = \sum_{i=0}^{359} y \sin^2(\theta) \quad (6d)$$

Finally, equation 6d was represented by the variable c_2 . Much like the similarity between Eq. 6c and Eq. 4d, Eq. 6d is very similar to Eq. 4c except the x has been replaced with a y and the $\sin^2 \theta$ term has replaced the $\cos^2 \theta$ term. The simplified version of Eq. 6 with all of the new variables introduced can now be established.

$$x b_2 + y c_2 = a_2 \quad (7)$$

Eq. 7 represents a much simpler version of Eq. 6. As was done in the previous section, the summation of $\sin \theta \cos \theta$ around a full rotation will give us zero, so the x terms will be cancelled out.

$$y = \frac{a_2}{b_2} \quad (7a)$$

Note that $a_1 = a_2$, eliminating the need to compute a_2 in the analysis. With all of the variables established for the x and y components, the simulation was then run using Excel.

Chapter 3

Data Generation and Analysis

Chapter 3 describes the steps leading up to the construction of the simulation and its use in generating results. The aim of this section is to describe how theoretical data was obtained using the equations derived in Chapter 2.

3.1 - Creating an Array for Rotation

The first step to gather information from the spreadsheet was to create an array to capture every possible angle of rotation of the rotor inside of the stator. As stated earlier, the angle of rotation of the rotor will be referred to by α . Each angle of α will be measured against every possible angle around the stator. The angle location on the stator will be referred to as θ . The array will be created to contain the form of $(\alpha - \theta)$. This allowed us to perform further calculations governed by the rotor's rotation through a complete turn in the stator.

| i | θ | α | | | | | | | |
|-----|----------|----------|---------------------|--------|--------|--------|--------|--------|--------|
| 0 | 0.000 | 0.000 | -0.017 | -0.035 | -0.052 | -0.070 | -0.087 | -0.105 | -0.122 |
| 1 | 0.017 | 0.017 | 0.000 | -0.017 | -0.035 | -0.052 | -0.070 | -0.087 | -0.105 |
| 2 | 0.035 | 0.035 | $(\alpha - \theta)$ | 0.000 | -0.017 | -0.035 | -0.052 | -0.070 | -0.087 |
| 3 | 0.052 | 0.052 | 0.017 | 0.000 | -0.017 | -0.035 | -0.052 | -0.070 | -0.087 |
| 4 | 0.070 | 0.070 | 0.052 | 0.035 | 0.017 | 0.000 | -0.017 | -0.035 | -0.052 |
| 5 | 0.087 | 0.087 | 0.070 | 0.052 | 0.035 | 0.017 | 0.000 | -0.017 | -0.035 |
| 6 | 0.105 | 0.105 | 0.087 | 0.070 | 0.052 | 0.035 | 0.017 | 0.000 | -0.017 |
| 7 | 0.122 | 0.122 | 0.105 | 0.087 | 0.070 | 0.052 | 0.035 | 0.017 | 0.000 |
| 8 | 0.140 | 0.140 | 0.122 | 0.105 | 0.087 | 0.070 | 0.052 | 0.035 | 0.017 |
| 9 | 0.157 | 0.157 | 0.140 | 0.122 | 0.105 | 0.087 | 0.070 | 0.052 | 0.035 |
| 10 | 0.175 | 0.175 | 0.157 | 0.140 | 0.122 | 0.105 | 0.087 | 0.070 | 0.052 |
| 11 | 0.192 | 0.192 | 0.175 | 0.157 | 0.140 | 0.122 | 0.105 | 0.087 | 0.070 |
| 12 | 0.209 | 0.209 | 0.192 | 0.175 | 0.157 | 0.140 | 0.122 | 0.105 | 0.087 |
| 13 | 0.227 | 0.227 | 0.209 | 0.192 | 0.175 | 0.157 | 0.140 | 0.122 | 0.105 |
| 14 | 0.244 | 0.244 | 0.227 | 0.209 | 0.192 | 0.175 | 0.157 | 0.140 | 0.122 |
| 15 | 0.262 | 0.262 | 0.244 | 0.227 | 0.209 | 0.192 | 0.175 | 0.157 | 0.140 |
| 16 | 0.279 | 0.279 | 0.262 | 0.244 | 0.227 | 0.209 | 0.192 | 0.175 | 0.157 |
| 17 | 0.297 | 0.297 | 0.279 | 0.262 | 0.244 | 0.227 | 0.209 | 0.192 | 0.175 |
| 18 | 0.314 | 0.314 | 0.297 | 0.279 | 0.262 | 0.244 | 0.227 | 0.209 | 0.192 |
| 19 | 0.332 | 0.332 | 0.314 | 0.297 | 0.279 | 0.262 | 0.244 | 0.227 | 0.209 |

Table 3-1: Rotation array creation in Excel.

Table 3-1 shows how the rotation data were generated as an input for the governing equations derived in Chapter 2. It captures only a small snapshot as the data will be in the form of a 360x360 matrix. The column on the far left shows the values for i used as a reference for the summations described previously in Chapter 2. θ was defined vertically and α was defined horizontally.

3.2 - Summation of $R(\theta)\cos\theta$ and $r(\alpha-\theta)\cos\theta$

The second step in the data analysis required calculation of the summations derived in Chapter 2. The summation of $R(\theta)\cos\theta$ was relatively easy to calculate because there was only one column that needs to be summed. The summation of $r(\alpha-\theta)\cos\theta$ was much larger than the

previous calculation because each rotation needed to be accounted for. There were 360 columns that were each summed up to gather the data required for a full rotation of the rotor within the stator.

| $R(\theta)*\cos(\theta)$ | $r(\theta-\alpha)*\cos(\theta)$ | | | | | |
|--------------------------|---------------------------------|--------|--------|--------|--------|--------|
| 0 | 0.000 | -0.087 | -0.174 | -0.259 | -0.342 | -0.422 |
| 0.087142469 | 0.087 | 0.000 | -0.087 | -0.173 | -0.259 | -0.342 |
| 0.173542396 | 0.174 | 0.087 | 0.000 | -0.087 | -0.173 | -0.259 |
| 0.258464343 | 0.258 | 0.174 | 0.087 | 0.000 | -0.087 | -0.173 |
| 0.341186999 | 0.341 | 0.258 | 0.173 | 0.087 | 0.000 | -0.087 |
| 0.421010072 | 0.421 | 0.341 | 0.258 | 0.173 | 0.087 | 0.000 |
| 0.497260948 | 0.497 | 0.421 | 0.340 | 0.258 | 0.173 | 0.087 |
| 0.569301085 | 0.569 | 0.497 | 0.419 | 0.340 | 0.257 | 0.173 |
| 0.636532045 | 0.637 | 0.568 | 0.495 | 0.419 | 0.339 | 0.256 |
| 0.698401123 | 0.698 | 0.635 | 0.567 | 0.494 | 0.418 | 0.338 |
| 0.754406507 | 0.754 | 0.697 | 0.633 | 0.565 | 0.493 | 0.416 |
| 0.804101914 | 0.804 | 0.752 | 0.694 | 0.631 | 0.563 | 0.491 |
| 0.847100671 | 0.847 | 0.801 | 0.749 | 0.692 | 0.629 | 0.561 |
| 0.883079177 | 0.883 | 0.844 | 0.798 | 0.746 | 0.689 | 0.626 |
| 0.911779734 | 0.912 | 0.879 | 0.840 | 0.795 | 0.743 | 0.686 |
| 0.933012702 | 0.933 | 0.908 | 0.875 | 0.837 | 0.791 | 0.740 |
| 0.946657971 | 0.947 | 0.929 | 0.903 | 0.871 | 0.833 | 0.788 |
| 0.952665728 | 0.953 | 0.942 | 0.924 | 0.899 | 0.867 | 0.828 |
| 0.951056516 | 0.951 | 0.947 | 0.937 | 0.919 | 0.894 | 0.862 |

Table 3-2: $R(\theta)\cos\theta$ and $r(\alpha-\theta)\cos\theta$

Table 3-2 shows a small glimpse of the data used to calculate each function representing the radius of the stator as $R(\theta)$ and the radius of the rotor $r(\alpha-\theta)$. The summations were performed at the bottom of the spreadsheet beneath the intermediate results shown in Table 3-2. These results will be discussed in greater detail in Chapter 4.

3.3 - Summation of Assorted Trigonometric Functions

The final step in the data sheet was to create a reference block that would represent equations 4c, 4d, 6c, and 6d. Starting first with Eq. 4c,

$$b_1 = \sum_{i=0}^{359} x \cos^2 \theta = \frac{n}{2} \quad (4c)$$

The sum of $\cos^2 \theta$ for a full rotation around a circle can be found to be $\frac{n}{2}$ with n being 360 for a full rotation; we are given the value of 180 to be used in Eq. 5a. Eq. 4d (which has the identical function as Eq. 6c), also receives a value of 0 because of the summation of sine and cosine products around a circle. Eq.4d is shown below as a quick reference.

$$c_1 = \sum_{i=0}^{359} y \sin \theta \cos \theta = 0 \quad (4d)$$

Finally, the last summation comes from Eq. 6d.

$$c_2 = \sum_{i=0}^{359} y \sin^2 \theta = \frac{n}{2} \quad (6d)$$

Much like the summation found in Eq. 4c, the sum of $\sin^2 \theta$ around a complete circle is well known to be $\frac{n}{2}$.

Chapter 4

Discussion of Results

The results were interpreted within the Excel sheet that was described in Chapter 3. All results were generated within the sheet based on the user input of the lobe design for the rotor and stator. The calculations are displayed immediately after entering the desired information. Plots showing the position of the center of the spindle were generated to allow an immediate visual representation of results. However, due to an unanticipated finding that was much simpler than the expected results, virtually eliminate the need for extensive plotting. Chapter 4 describes the simulation results and their use in explaining the smoothing effect that has long been observed in air bearing spindles.

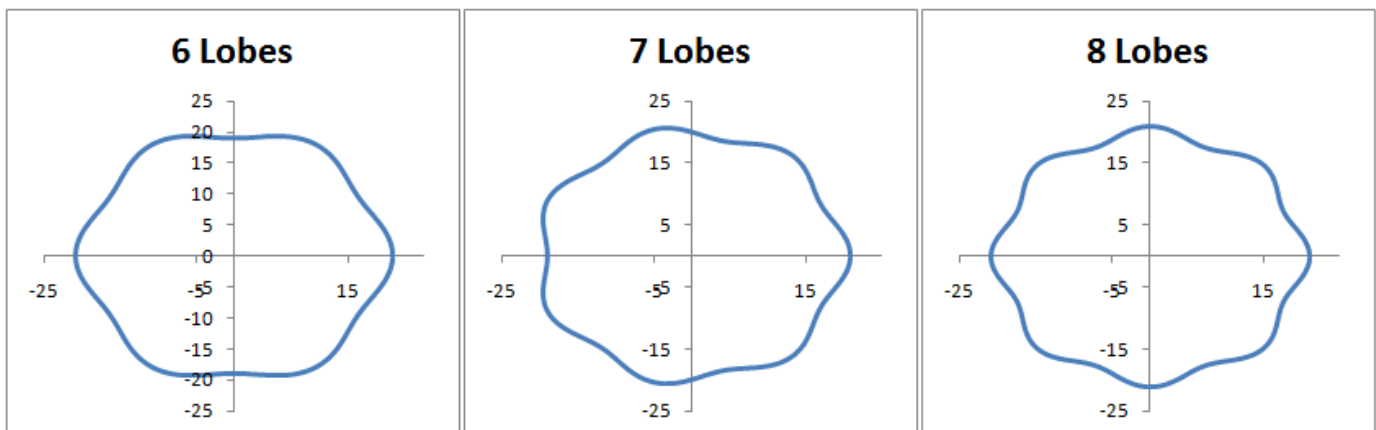


Figure 4-1: Stator design with multiple lobes.

Fig. 4-1 shows the form error of a stator with various lobe manufacturing designs. The amplitude of the lobes is grossly exaggerated to illustrate the actual shape of the stator.

4.1 - Summation Calculations

As previously discussed, there are three summations in each of the governing equations for the x and y components for the center of the spindle. Looking at the x components first, Eq. 5a must be solved to obtain the x components. Eq. 5a had been shown as a smaller representation, but we must look back at the original equation for the numerator to understand the results properly.

$$\sum_{i=0}^{359} R(\theta) \cos \theta - \sum_{i=0}^{359} r(\theta - \alpha) \cos \theta \quad (4b)$$

Eq. 4b is the numerator found in Eq. 5a. After performing all of the calculations within the spreadsheet for different combinations of lobe designs, it emerged that regardless of the combination of lobes on both the rotor and stator that the objective function's summation around the entire revolution of the rotor inside the stator can be zero if both x and y are zero. This means that the theoretical spindle error motion is zero regardless of the number of lobes on either the rotor or the stator.

The objective at the beginning of this investigation was to calculate the position of a spindle's axis of rotation given different inputs for lobe shapes in the rotor and stator. The results show that within the limits of the assumptions made in the representation of the air film as a linear spring, that the x and y components were found to always equal zero. These results are extremely helpful in explaining the huge averaging effect that is known to occur in externally-pressurized air bearing spindles.

4.2 - Non-linear Spring Behavior

One of the major assumptions that were made throughout this investigation was that the air inside the spindle acted as a linear spring with constant k . This assumption seemed to be reasonable in order to test whether designs for manufacturing could influence accuracy of the spindle. If the behavior of the spring is not linear, the calculations become much more difficult. The spring constant dropped out of the simulation after taking the derivative of Eq. 3 and some further simplification. However, if the stiffness of the air film acted in a non-linear fashion, the terms would still be present throughout the entire calculation process. The nature of the spring constant from the air can be influenced by small grooves found in the spindle that allow air flow during operation. These grooves are very small, but may lead to a non-linear stiffness behavior of the spindle. In order to correctly model this in the simulation, further research should be done in order to determine a reasonable non-linear model to represent the air film's stiffness.

4.3 - Load of Air Bearing

The pressurized air film has been shown to offer a significant smoothing effect on the accuracy of the rotating spindle. With rotor and stator form errors on the order of 0.25 to 0.5 μm , the air film absorbs essentially all of this during spindle operation. The error motion of an actual spindle is known to be as low as 5nm. This means that pressurized air film inside the bearing acts in a manner that dramatically reduces the effects of inaccuracies during spindle operation. In retrospect, this makes sense because the load that the air exerts on the rotor and stator is designed to minimize surface defects and factors that influence accuracy. Lobing in the rotor and stator would be nearly cancelled out by the forces of the air as the spindle speed is increased. This can

also be attributed to the spring behavior of the spring from the previous discussion. Our analysis was based on the idea that a linear spring would be attached every one degree around the rotor.

4.4 - Further Recommendations

There is still a large amount of analysis that can be conducted to predict the tiny residual (nanometer-level) inaccuracies that are observed in high precision air bearing spindles. The determination of a more accurate model for the spring behavior of the air during operation may prove to be helpful in accurately predicting the performance of a spindle. Determining any nonlinear spring stiffness will help to generate an objective function that can be implemented into Eq. 3. The non-linear behavior will complicate the mathematics heavily, but the simulation should be able to capture the changes to the spring constant. After the spring constant is determined, the load characteristics of the air bearing can be understood more fully. The air allows for correction of current surface defects on the rotor and stator, but a better understanding of how effectively the air corrects these flaws can be achieved. Finally, if these previous two characteristics can be determined, the process of predicting the effect of lobes in the rotor and stator could be physically tested. By refining the assumptions made about the behavior of the air, simulations may increase in accuracy to the point that even the small residual error may be predicted.

4.5 - Conclusion

This work presents a comprehensive model and simulation that demonstrates how the well-known accuracy of externally-pressurized air bearing spindles is possible, even in the presence of

significant manufacturing errors in the rotor and stator. The effects of form errors (geometric flaws) in the rotor and stator are shown to have no first-order effect on the spindle error motion. The results provide insight into why high precision air bearing spindles achieve such remarkable accuracy due to the smoothing effect of the air film.

References

- ANSI/ASME, "Methods for Specifying and Testing," *Axes of Rotation*, An American National Standard, B89.3.4-2021
- D. Schalcosky, *Design of a precision parallel axis flatness inspection machine*, Master's Thesis: The Pennsylvania State University, 2002.
- E. Marsh, *Precision Spindle Metrology*, Lancaster, PA: DEStech Publications, 2010, p. 1-37.
- E. Marsh, D. Yantek, "Experimental measurement of precision bearing stiffness," *Journal of Sound and Vibration*, Vol. 202, 55-66, 1997.
- E. R. Marsh and D. L. Marting, "Instrumented air bearing spindle for precision grinding," *Proceedings of the Intl Conf on Precision Engineering*, Vol. 24, 50-57, 1997.
- E. Marsh, J. Couey, R. Vallance, "Nanometer-level comparison of three spindle error motion separation techniques," *ASME Journal of Manufacturing Science and Engineering*, Vol. 128, 180-187, 2006.
- G. K. Arora et al, "Measurement and evaluation of spindle running error," *International Journal of Machine Tool Design Research*, Vol. 17, 127-135, 1977.
- H. Jhansale, D. Mccann, "Condition Assessment and Improvement of a Steam Turbine Rotor," *Handbook of Case Histories in Failure Analysis*, Vol. 1, 1992.
- J. E. Bibler, *Effects of imbalance and geometric error on precision grinding machines*, Master's Thesis: Berkeley, 359-364, 1997.
- P. Smith, R. Vallance, E. Marsh, "Correcting capacitive displacement measurements in metrology applications with cylindrical artifacts," *Precision Engineering*, Vol. 29, 324-335, 2005.
- R. Grejda, *Use and calibration of ultra-precision axes of rotation with nanometer level metrology*, PhD Thesis: The Pennsylvania State University, 2002.
- S. Wu, J. Ni, "Precision machining without precise machinery," *Annals of CIRP*, Vol. 38, 533-536, 1989.
- T. Murthy, C. Mallanna, M. Visveswaran, "New methods of evaluating axis of rotation error," *Annals of CIRP*, Vol. 27, 365-369, 1978.

James R. Nevel

Permanent Address
5107 Wolf Run Drive
Erie, PA 16505

School Address
212 West Fairmount Avenue
State College, PA 16801

Education: **Pennsylvania State University, Schreyer Honors College** – *University Park, PA*
(2007 – Present) B.S. expected in May of 2011 Major: Mechanical Engineering

Relevant Coursework: Multiple levels of Calculus, Statics, Strength of Materials, Thermodynamics, Dynamics, Fluid Mechanics, Mechanical Design, System Controls

Related Experience: **GE Transportation** – *Erie, PA*

Summer 2010 – Simulation Team

- Enhanced communication with different disciplines of engineering (electrical, software, computer)
- Contributed to the development and set-up of the CAX simulator to increase testing productivity
- Gained experience using Labview in order to develop visual coding for simulation testing

Summer 2009 – Drivetrain Technologies

- Created a tolerance stack up for the interaction among all subsystems in a new gearbox design.
- Tracked weight and cost CTQs at a system and subsystem level for a new customer.
- Presented limitations for gearbox maintainability through analysis of multiple system interactions.
- Conducted research on environmental / international standards surrounding wind turbines.

Summer 2008 – Drivetrain Technologies

- Created a summarized scorecard determining traceability of CTQs in an SLE gearbox.
- Maintained customer focus by working with an FMI solution to increase gearbox reliability.
- Kept production and designs moving forward with open action item updates.
- Created headcount summary to maximize resource allocation for current and upcoming projects.

Awards: Valedictorian, Class of 2007
Schreyer Honors College Scholarship, 2007-2011
GE Star Scholarship
Eagle Scout, Boy Scouts of America

Activities:

Penn State Dance MaraTHON Rules & Regulations Captain, 2011
Atlas THON Fundraising Co-Chair, 2010
Penn State Dance MaraTHON Supply Logistics Captain, 2010
Atlas THON Recruitment Captain, 2009
Penn State Dance MaraTHON Supply Logistics Captain, 2009
Pentagon Paintball Team, 2007 - *Captain*
JETS Engineering Team, 2006-2007
Pennsylvania Junior Academy of Science (3 years)